The Influence of Geomagnetic Disturbance on Transient Power Angle Stability of Hybrid Systems

Si, Yuan; Wang, Zezhong ; Liu, Lianguang ; Anvari-Moghaddam, Amjad

Published in:
2022 IEEE International Conference on Environment and Electrical Engineering and 2022 IEEE Industrial and Commercial Power Systems Europe

DOI (link to publication from Publisher):
DOI: 10.1109/EEEIC/ICPSEurope54979.2022.9854729

Publication date:
2022

Document Version
Accepted author manuscript, peer reviewed version

The Influence of Geomagnetic Disturbance on Transient Power Angle Stability of Hybrid Systems

Yuan Si
School of Electrical & Electronic Engineering
North China Electric Power University
Beijing, China
ysi@energy.aau.dk

Zezhong Wang
School of Electrical & Electronic Engineering
North China Electric Power University
Beijing, China
wzzh@ncepu.edu.cn

Lianguang Liu
School of Electrical & Electronic Engineering
North China Electric Power University
Beijing, China
liulianguang@ncepu.edu.cn

Amjad Anvari-Moghaddam
Department of Energy
Aalborg University
Aalborg, Denmark
aam@energy.aau.dk

***Abstract*—The reactive power loss of transformers (hereinafter referred to as GIC-Q) caused by geomagnetically induced current (GIC) has the characteristics of large total amount and strong fluctuation. As a kind of reactive load added to the system, GIC-Q can cause the change of operating state. The influence of geomagnetic disturbance (GMD) on system stability focuses on the static stability of conventional systems, and its influence on the transient stability of hybrid systems has not been studied. This study establishes the random fuzzy model of induced geoelectric field components and calculates the expected values of critical clearing angle and acceleration/deceleration area. And the transient stability margin is quantitatively analyzed considering the influence of GMD. The result shows that GMD deteriorates the transient stability of the system, and the transient stability margin is the smallest when the wind power access ratio is about 50%. The research results provide a basis for disaster prevention and control of GMD.**

Keywords—Fuzzy simulation, geomagnetic disturbance, GIC-Q, Hybrid system, transient stability

I. INTRODUCTION

Geomagnetically induced current (GIC) (0.1Hz or lower) is generated in the power system driven by geomagnetic disturbance (GMD). GIC flows through the transformer making its core half-wave saturated to generate reactive power loss (GIC-Q) [1,2], harmonic and vibration temperature rise [3], which affects the safe and stable operation of the system. At present, the research on the influence of GMD on the system mainly focuses on voltage stability and does not consider wind power access.

Concerning the induced geoelectric field data in the analysis of the impact of GMD on system stability, references [4] and [5] respectively use the amplitude of induced geoelectric field in a geomagnetic storm event or the assumed value of 1V/km to study the impact of GMD on voltage stability. However, only using the induced geoelectric field amplitude to analyze the risk of system instability caused by GMD may cause the evaluation result to be higher than the actual value, and the influence of GMD on system stability cannot be comprehensively analyzed. Reference [6] analyzed the induced geoelectric field and GIC statistical law generated by multiple GMDs in the 23rd solar activity cycle. Given the uncertainty of GMD, it is necessary to propose an induced geoelectric field model that can comprehensively describe its randomness and fuzziness.

The GIC-Q caused by GMD is the main reason threatening the stable operation of the system. The impact of GIC-Q on voltage stability has been studied in [7,8] and the concept of GMD-electrical hybrid simulation has been proposed in [9]. But the research direction of these studies have been focused on conventional systems and do not consider the role of renewables (such as wind-dominated power systems) in the current energy mix and their impact on anti-GMD ability of the system. Reference [10] valuated the assumption of linear superposition in the context of GMD calculations, the k-factor method, and the impact of GMD-related system dynamics on voltage stability results. In fact, the change of GIC-Q caused by the change of network topology during normal operation, fault and after fault removal is not considered. GIC-Q, as an uncertain reactive power load, can cause the change of operation state in the system. Whether it will affect the transient stability of the system and how to quantitatively evaluate this impact remain to be further studied.

In this paper, the induced geoelectric field component is calculated by using the multiple GMD data in the 23rd solar activity cycles and the plane wave method [11], and its probability distribution characteristics are extracted. Then, the fuzzy membership of probability distribution function (PDF) parameters is defined. Based on the uncertainty theory, the induced geoelectric field is defined as a random fuzzy variable and its opportunity measure distribution function is obtained, so a random fuzzy model of induced geoelectric field is proposed. The equivalent grounding impedance is used to replace GIC-Q and wind power output. Through matrix deflation, GMD is connected with inertia, mechanical power and electromagnetic power in the equivalent rotor motion equation of extended single machine-infinite bus system. The expected value of critical clearing angle, acceleration/deceleration area and transient stability margin under the influence of GMD is obtained by fuzzy simulation calculation, and the influence of GMD on the transient power angle stability of the hybrid system is quantified, which provides a basis for the treatment of geomagnetic storm disasters.

This work was supported in part by the National Key Research and Development Plan under Grant 2016YFC0800103, in part by the National Natural Science Foundation of China under Grant 50677060.

II. ANALYSIS OF RANDOM FUZZINESS OF INDUCED GEOELECTRIC FIELDS

A. Probability distribution characteristics of induced geoelectric fields

In order to quantitatively compare the fitting effect of each PDF of induced geomagnetic fields, a fitting index is defined, as shown in (1).

$$I = \sum_{i=1}^{M} (y_i - \overline{N_i}) \tag{1}$$

where M is the number of groups of frequency distribution histogram; $y_i = f\left(\overline{C_i}\right)$, $\overline{N_i}$ and $\overline{C_i}$ are the height and center position of the *i*-th straight square column respectively; $f(\cdot)$ is the fitted PDF; y_i is the value corresponding to the fitting probability density function at the center position $\overline{C_i}$. The smaller the fitting index *I*, the higher the fitting accuracy.

The induced geomagnetic field components of 29 geomagnetic storms are fitted by the normal distribution, Cauchy distribution, and t location-scale distribution. As another expression of the t distribution, the PDF of the three-parameter t distribution is $pdf\left(E_{x/y}, \mu_{x/y}, \sigma_{x/y}, \upsilon_{x/y}\right)$, where $\mu_{x/y}$ is the position parameter, $\sigma_{x/y}$ is the scale parameter, $\upsilon_{x/y}$ is the shape parameter. The average value of mean squared error of East-West component E_x is 0.851, 0.318 and 0.116, the maximum is 0.893, 0.379 and 0.225, and the minimum is 0.802, 0.203 and 0.107. The average value of mean squared error of North-South component E_y is 0.556, 0.591 and 0.211, the maximum is 0.658, 0.671 and 0.336, and the minimum is 0.421, 0.502 and 0.159. The fitting effect of t location-scale function is the best, so it is used to fit the distribution of E_x and E_y.

B. Fuzzy analysis of probability distribution parameters of induced geoelectric fields

The frequency statistics of PDF parameters of induced geoelectric fields are carried out according to the interval, and the frequency distribution of parameters is obtained. Triangular function and trapezoidal function are used to represent $\mu_{x/y}$, $\sigma_{x/y}$ and $\upsilon_{x/y}$. For the PDF parameter of E_x, the value of μ_x is approximately centered on 6.911. With the gradual increase of the distance from the center, the occurrence frequency of its value shows a downward trend except for some special points. If considering excluding the influence of special parameter values, μ_x can be approximately described by triangular fuzzy variables. The membership function types and parameters are also obtained according to the distribution law of μ_y, σ_y and υ_y, as shown in Table I, where μ_x, $\sigma_{x/y}$, $\upsilon_{x/y}$ are represented by triangular fuzzy numbers, μ_y is represented by trapezoidal fuzzy number.

TABLE I
MEMBERSHIP FUNCTION OF PDF PARAMETERS

Parameters	Parameters of fuzzy number			
	a	***b***	***c***	***d***
μ_x	3.042	6.911	11.100	-
σ_x	2.304	3.957	7.263	-
υ_x	1.250	1.845	3.929	-
μ_y	8.902	13.440	20.261	29.340
σ_y	6.869	11.760	21.532	-
υ_y	1.262	1.866	3.989	-

The random variable distribution types of E_x and E_y are determined, and their parameters are described as fuzzy variables. The random fuzzy variables ξ_{E_x} and ξ_{E_y} are used to represent E_x and E_y, and the chance measure distribution function of t location-scale distribution is shown in (2).

$$F_{x/y}\left(\xi_{E_{x/y}}\right) = Ch(E_{x/y} < \xi_{E_{x/y}}) \tag{2}$$

where $F(\cdot)$ is cumulative probability density function (CDF). $Ch(\cdot)$ is chance measure operator.

C. Random fuzzy simulation method of induced geoelectric fields

Random fuzzy simulation technology and inverse transformation method are used to generate induced geoelectric field samples. The specific steps are as follows:

1) Based on the chance measure distribution function of induced geoelectric fields, M parameter samples of $P_{os}\{\cdot\} \geq \varepsilon$ are extracted from the confidence intervals of parameters $\mu_{x/y}$, $\sigma_{x/y}$, and $\upsilon_{x/y}$, where P_{os} is the possibility measure and ε is a sufficiently small positive number.

2) The extracted M μ_{xi}, σ_{xi}, υ_{xi} $(i = 1, 2, \cdots, m)$ are matched into corresponding combinations, and the values of $P_{os}\left\{\mu_{xi}, \sigma_{xi}, \upsilon_{xi}\right\}$ are generated by simulation in the interval [0,1].

3) The parameter combination obtained in Step 2) is taken as the t location-scale parameter, and the inverse function of (5) is solved to obtain the value $\xi_{E_{xi/yi}} = F_x^{-1}\left[Ch(E_{x/y} < \xi_{E_{xi/yi}})\Big|_{(\mu_{xi/yi}, \sigma_{xi/yi}, \upsilon_{xi/yi})} \right]$ of the induced geoelectric field. The possibility of the occurrence of the induced geoelectric field component is the possibility measure $P_{os}\left\{\mu_{xi}, \sigma_{xi}, \upsilon_{xi}\right\}$ of the combination of $\left\{\mu_{xi}, \sigma_{xi}, \upsilon_{xi}\right\}$, denoted by $v_{xk} = P_{os}\left\{\mu_{xi}, \sigma_{xi}, \upsilon_{xi}\right\}$, $v_{yk} = P_{os}\left\{\mu_{yi}, \sigma_{yi}, \upsilon_{yi}\right\}$.

4) The induced geoelectric field components $\xi_{E_{xi}}$ and $\xi_{E_{yi}}$ are randomly combined into induced geoelectric field $\left(\xi_{E_{xi}}, \xi_{E_{yi}}\right)$, and its possibility measure v_k is $v_{xk} \cdot v_{yk}$.

In practical operation, since the specific expression of the inverse function cannot be given directly, the graphical method is used for calculation, that is, the CDF curve is obtained by using the parameter sample $\left\{\mu_{xi}, \sigma_{xi}, \upsilon_{xi}\right\}$, the horizontal axis is the size of E_x, the vertical axis is the probability density. The point $P_{os}\left\{\mu_{xi}, \sigma_{xi}, \upsilon_{xi}\right\}$ on the

vertical axis is known, and the corresponding $\xi_{E_{xi}}$ is found. The acquisition method of $\xi_{E_{yi}}$ is the same.

III. ANALYSIS OF GMD ON SYSTEM TRANSIENT STABILITY

A. Equivalent model of wind farm power output and GIC-Q

According to the extended equal area criterion (EEAC), the synchronous generators can be divided into two groups, leading group S and remaining group R. The extended dual-machine system is shown in Fig. 1. All nodes in the system are divided into four categories: potential node S in S-group synchronizer (node 1) and potential node R in R-group synchronizer (node 2), wind farm access node W (node 3) and load node L in the network (nodes 4, 5, 6 and 7).

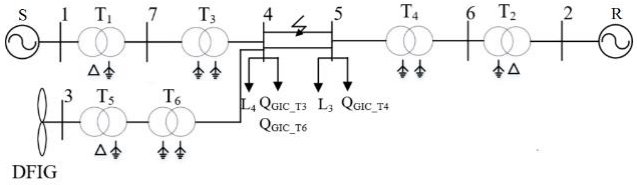

Fig. 1. Wiring diagram of an extended dual-machine system

In the case of GMD, the potential difference occurs at the grounding points of transformers in different geographical locations, which forms a loop through the ground and transmission lines to generate GIC. Half-wave saturation occurs when GIC flows through the transformer, and the reactive power loss of the transformer increases. This part of reactive power loss is added to the system as reactive loads.

Whether it is normal operation, short-circuit fault or fault removal, GIC-Q can be used as a reactive load, but its size changes with the change of GMD intensity and network topology. Therefore, GIC-Q can be equivalent to a positive reactance, as shown in (3).

$$X_{Q_{GICi}} = j\frac{Q_{GICi}}{U_{Q_{GICi}}^2} \tag{3}$$

where $X_{Q_{GICi}}$ is the reactance. $U_{Q_{GICi}}$ is the node voltage of the transformer node generating GIC-Q. Q_{GICi} is the reactive power loss caused by GIC flowing through the transformer, which is calculated by K-value method [12]. $i=1,2,3$ respectively represents normal, fault, and fault removal conditions.

Assuming that the wind farm access node W is inside the S-group, when the wind power access ratio is k_S, the active power output of the wind farm is $P_W = k_S P_{m.S0}$ and $P_{m.S0}$ is the mechanical power of the S-group. Under normal conditions, doubly-fed induction generator (DFIG) only provides active power to the system, which can be equivalent to a negative resistance R_{W1}. In the case of fault, DFIG terminal voltage drops. In order to recover the terminal voltage, DFIG with low voltage ride through capability sends reactive power to the system under the action of the control system. Therefore, DFIG is equivalent to a parallel negative resistance R_{W2} and negative reactance X_{W2}. After fault removal, DFIG not only generates active power, but also emits a small amount of reactive power. Therefore, DFIG is equivalent to a negative impedance with negative resistance R_{W3} and negative reactance X_{W3} in parallel. The equivalent impedance is shown in (4), (5).

$$R_{Wi} = \frac{U_{Wi}^2}{P_{Wi}} (i=1,2,3) \tag{4}$$

$$X_{Wi} = \frac{U_{Wi}^2}{Q_{Wi}} (i=2,3) \tag{5}$$

where U_{Wi} is the voltage of DFIG access point. P_{Wi} and Q_{Wi} are the active power and reactive power of DFIG. $i=1,2,3$ respectively represent three states: normal, fault and fault removal.

When GMD occurs and wind power output changes, the self-admittance Y_{44i_0} and Y_{55i_0} of nodes 4 and 5 are corrected to Y_{44i} and Y_{55i}, $Y_{44i} = Y_{44i\_0} + 1/Z_{Wi} + 1/X_{Q_{GICi}}$, $Y_{55i} = Y_{55i\_0} + 1/X_{Q_{GICi}}$, where Y_{44i_0} and Y_{55i_0} are the self-admittance of nodes 4 and 5 without GMD and wind farm respectively. According to the node classification, the node voltage equation of system (6) is obtained by eliminating nodes 3, 4, 5, 6 and 7.

$$\begin{pmatrix} Y_{11} - \Delta f_1(k_S, Q_{GIC}) & Y_{12} - \Delta f_2(k_S, Q_{GIC}) \\ Y_{21} - \Delta f_3(k_S, Q_{GIC}) & Y_{22} - \Delta f_4(k_S, Q_{GIC}) \end{pmatrix} \begin{pmatrix} \boldsymbol{E}_1 \\ \boldsymbol{E}_2 \end{pmatrix} = \begin{pmatrix} \boldsymbol{I}_1 \\ \boldsymbol{I}_2 \end{pmatrix} \tag{6}$$

where $\Delta f_i(k_S, Q_{GIC})$ ($i=1,2,3,4$) is the correction of admittance. Because the expression of admittance correction is complex, it is expressed in function form.

B. Influence of GMD on equivalent rotor motion equation of the hybrid system

According to [13], it is assumed that wind power is connected to S-group, the equivalent inertia $M_S(k_S)$ and mechanical power $P_{m.S0}(k_S)$ is shown in (7).

$$\begin{cases} M_S(k_S) = (1-k_S) M_{S0} \\ P_{m.S}(k_S) = (1-k_S) P_{m.S0} \end{cases} \tag{7}$$

where M_{S0} is the equivalent inertia of the S-group without wind power access.

The rotor motion equations of equivalent synchronizers S and R are subtracted, and the extended two-machine system is equivalent to a single machine infinite bus system. By analyzing the influence of GMD and wind power access ratio on the moment inertia, mechanical power and electromagnetic power of synchronizer, the influence is reflected in the variation relationship between each parameter in the equivalent rotor motion equation and k_S, Q_{GIC}, as shown in (8).

$$M_{SR}(k_S)\ddot{\delta}_{SR} = P_{m.SR}(k_S) - P_{e.SR}(k_S, Q_{GIC}) \tag{8}$$

where M_{SR} is the equivalent inertial time constant. $P_{m.SR}$ and $P_{e.SR}$ are equivalent mechanical power and electromagnetic power respectively. Because the expression of parameters is complex, they are expressed in the form of k_S and Q_{GIC} functions.

It can be seen from (8) that the equivalent mechanical power and electromagnetic power of the system are affected

by k_S and GIC-Q. Therefore, the influence of GMD on the transient stability of hybrid system is transferred to the influence of k_S and GIC-Q on the acceleration/deceleration area.

C. Evaluation of the influence of GMD on transient stability

Using the induced geoelectric field samples obtained in section 1.3, the expected value of parameters related to system transient stability under the influence of GMD is calculated. The specific steps are as follows:

1) Combined with the power grid structure parameters and K-value method, M-group sampling values $\left(\xi_{E_{xi}}, \xi_{E_{yi}}\right)$ are calculated in turn to obtain the M-group GIC-Q sample of the substation.

2) Determine a certain wind power access proportion k_S, and calculate the critical clearing angle samples δ_c, acceleration area S_{ac} and deceleration area S_{dc} in combination with M-group GIC-Q. The minimum critical clearing angle, the minimum acceleration area and the minimum deceleration area are recorded as δ_{cmin}, S_{acmin} and S_{dcmin}. The maximum critical clearing angle, the maximum acceleration area and the maximum deceleration area are recorded as δ_{cmax}, S_{acmax} and S_{dcmax}.

3) r_δ, r_{ac} and r_{dc} are uniformly generated from $[\delta_{cmin}, \delta_{cmax}]$, $[S_{acmin}, S_{acmax}]$ and $[S_{dcmin}, S_{dcmax}]$, respectively. Let e_δ=0, e_{ac}=0, e_{dc}=0.

4) Perform M cycles for (9) and (10), and accumulate the e value in each cycle.

$$e_\delta = e_\delta + \frac{1}{2}\left(\max_{1\le k\le M}\{v_k \mid \delta_\delta \ge r_\delta\} + \min_{1\le k\le M}\{1-v_k \mid \delta_\delta < r_\delta\}\right) \quad (9)$$

$$e_{S_{ac/dc}} = e_{S_{ac/dc}} + \frac{1}{2}\left(\max_{1\le k\le M}\{v_k \mid S_{ac/dc} \ge r_{ac/dc}\} + \min_{1\le k\le M}\{1-v_k \mid S_{ac/dc} < r_{ac/dc}\}\right) \quad (10)$$

5) Calculate the expected value of the critical clearing angle $E[\delta_c] = \delta_{c\min} + e_\delta \times (\delta_{c\max} - \delta_{c\min})/M$. Calculate the expected value of acceleration/deceleration area $E[S_{ac/dc}] = S_{ac\min/dc\min} + e_{ac/dc} \times (S_{ac\max/dc\max} - S_{ac\min/dc\min})/M$.

The difference between deceleration area and acceleration area divided by acceleration area is defined as transient stability margin, as shown in (11).

$$\eta = \frac{S_{de} - S_{ac}}{S_{ac}} \times 100\% \quad (11)$$

where S_{ac} and S_{de} are the expected values of acceleration area and deceleration area respectively. η is the transient stability margin.

IV. Example Analysis

A. GIC-Q under normal operation and fault conditions

Taking the modified IEEE 118-Bus test case [14] as an example, the influence of GMD on the transient stability is analyzed. The transformers are numbered T_1~T_9 respectively according to the subsequence of their connected nodes. For the hybrid system, it is assumed that DFIG access node is node 8, and the rated power of a single DFIG is 1.5 MW. The number of DFIGs in the wind farm changes according to the wind power access capacity.

It is assumed that a three-phase short-circuit fault occurs at the midpoint of branch 30-38 at t=1s, and the fault is removed at 1.3s. By switching synchronous units to accept wind power, the inertia constant of the multi-machine system is changed, and then the clustering result of the multi-machine system is changed. According to the identification method of coherent generator group in [15], the clustering result of coherent generator group is obtained.

Since the data collected from the geomagnetic station are GMD second data and the fault duration is short, it is considered that the GMD intensity remains unchanged during the fault. Taking E_x = 0.8 V/km, E_y = 0.4 V/km as an example, the GIC-Q of 9 substations during normal operation, fault and fault removal are shown in Table II.

TABLE II
GIC-Q OF EACH SUBSTATION

Substation	GIC-Q(MVar)			Difference/%
	Normal operation	*Fault*	*Fault removal*	
1	14.9	10.0	20.3	32.8(36.2)
2	58.9	45.2	67.5	23.1(14.5)
3	128.9	149.5	108.6	16.0(15.6)
4	48.1	43.0	41.0	10.7(14.8)
5	53.2	64.2	47.3	20.5(11.0)
6	17.5	25.6	25.1	46.6(43.5)
7	75.8	72.1	51.6	4.8(31.8)
8	36.6	48.9	45.6	33.5(24.5)
9	42.8	34.6	50.3	19.0(17.5)

Note: the results outside the brackets are the changing rate when the fault occurs compared with normal operation. The results inside the brackets are the changing rate when the fault remove compared with normal operation.

Comparing the GIC-Q of each substation in three cases, it can be seen that the change of network topology can change the flow path of GIC, and then affect the size of GIC-Q. Therefore, the GIC-Q of each substation in three cases and the corresponding node voltage are used to calculate the equivalent impedance. Considering the change of node voltage during the fault, the average value of equivalent impedance is used to study the influence of GMD on transient stability.

For a GMD intensity, after the normal operation and fault removal, substitute the DFIG output active and reactive power and DFIG access node voltage into (4) and (5), and calculate the corresponding DFIG equivalent grounding impedance. When a fault occurs, due to the change of node voltage, the average value during the fault period is used to reflect the equivalent grounding impedance parameter of DFIG output power. Under different GMD intensities, the equivalent node impedance corresponding to three cases is calculated by using multiple groups of induced geoelectric field samples.

B. Influence of GMD on transient stability

For the conventional system, that is, when k_S=0, the critical clearing angle of the system is 113.56°. According to the statistics of induced geoelectric fields in 29 strong geomagnetic storm events, the variation range of E_x is -1~1 V/km, and the variation range of E_y is -0.4~0.4 V/km. Here, this induced geoelectric field component is taken as the limit and the GIC-Q is calculated in steps of 0.1V/km. After the GIC-Q is equivalent to the grounding impedance, the random of GMD makes the change of critical clearing angle irregular. But compared to the situation where there is no GMD, the critical clearing angle decreases, so the stability becomes worse.

For the case of $k_S \neq 0$, the critical clearing angle and its partial derivative to k_S are calculated. Using the random fuzzy simulation technology and inverse transformation method described in Section II-C, set M to 100 to generate induced geoelectric field samples. Then, for each k_S and multiple groups of induced geoelectric field samples, the expected value of the critical clearing angle is calculated by using Section III-C fuzzy simulation, and the variation law of the critical clearing angle with the proportion of wind power is obtained, as shown in Fig. 2.

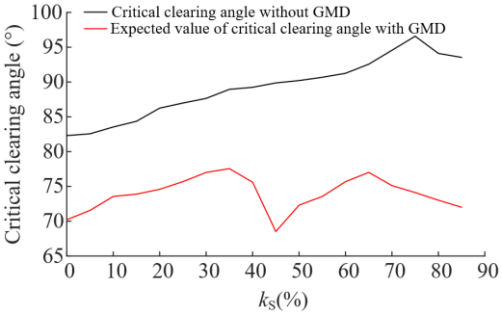

(a)

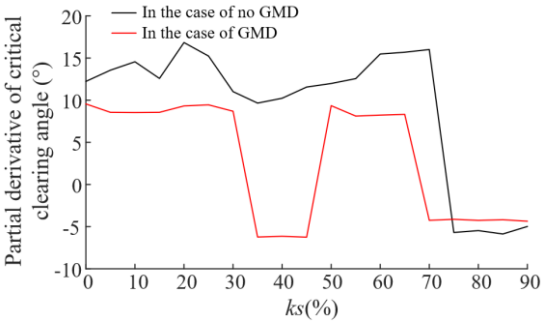

(b)

Fig. 2. Critical clearing angle. (a) Partial derivative of critical clearing angle to k_S. (b) Critical clearing angle of different k_S.

For the case without GMD, when k_S is in the range of 0~70%, $\frac{\partial \delta_c}{\partial k_S}$ is greater than zero. Therefore, the critical clearing angle increases with the increase of wind power proportion. When k_S is greater than 70%, $\frac{\partial \delta_c}{\partial k_S}$ is less than zero, so the critical clearing angle decreases with the increase of wind power proportion. When GMD occurs, the changing trend of critical clearing angle is more complex. The critical clearing angle increases first, then decreases, then increases and finally decreases with the increase of k_S, but compared to the case without GMD, the critical clearing angle decreases. Therefore, GMD is not conducive to transient stability.

The influence of GMD on acceleration/deceleration area is shown in Fig.3. The power characteristics of normal operation, fault and fault removal are represented by P_{I}, P_{II}, P_{III}, and black curves are the power characteristics without GMD. The uncertainty of GMD makes the electromagnetic power of the equivalent system not a fixed curve, but a cluster of red curves. The blue curves are envelopes of electromagnetic power during normal operation in the case of GMD. The cyan curves are envelopes of electromagnetic power in case of fault and GMD. The green curves are envelopes of electromagnetic power after the fault is removed.

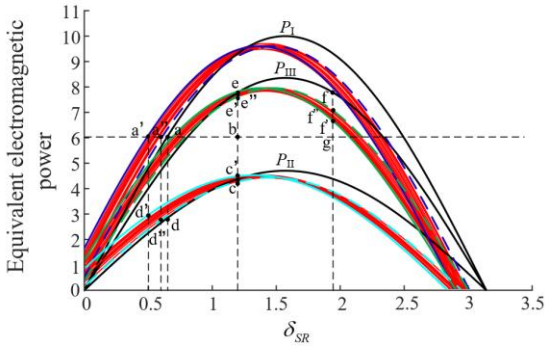

(a)

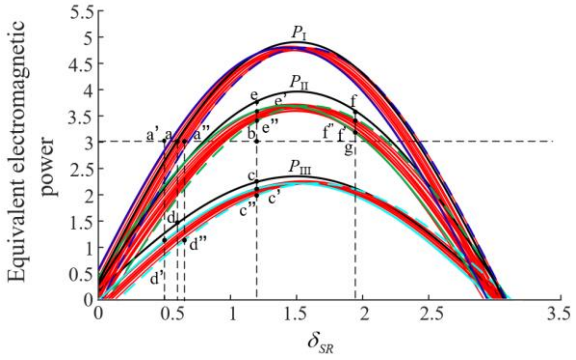

(b)

Fig. 3. Equivalent electromagnetic power curve. (a) k_S=0%. (b) k_S=40%.

S_{abcd} in Fig.3 is the acceleration area without GMD, $S_{a'bc'd'}$ and $S_{a'bc'd'}$ are the acceleration area composed of the envelope of equivalent electromagnetic power curve when GMD occurs, and the change of acceleration area cannot be obtained directly. S_{efgb} is the deceleration area without GMD, and $S_{e'f'gb}$ and $S_{e'f'gb}$ are the deceleration area composed of the envelope of the equivalent electromagnetic power curve when GMD occurs. The deceleration area decreases when GMD occurs in both conventional systems and hybrid systems. The S_{ac}, S_{dc} and η in case of GMD and no GMD under different wind power access ratios are shown in Table III.

TABLE III
THE EXPECTED VALUE OF ACCELERATION/DECELERATION AREA AND STABILITY MARGIN UNDER DIFFERENT WIND POWER RATIO

k_S(%)	S_{ac}	S_{de}	η/%
0	83.1(114.1)	114.1(112.0)	37.2(24.3)
10	80.0(85.4)	113.0(110.0)	41.2(28.7)
20	88.6(93.2)	121.5(112.6)	37.1(20.7)
30	86.9(87.7)	125.9(124.5)	44.8(41.9)
40	83.0(88.7)	127.0(120.5)	53.0(35.7)
50	80.3(90.6)	128.3(122.5)	59.6(35.2)
60	78.0(88.8)	130.0(125.7)	66.5(41.4)
70	77.3(88.7)	131.0(124.3)	69.3(40.1)
80	78.8(88.9)	130.7(124.0)	65.6(39.4)
90	79.0(90.7)	129.6(124.7)	64.0(37.4)

Note: the results outside the brackets are the results without GMD, and the results inside the brackets are the results when GMD occurs.

Without GMD, the transient stability margin increases with the increase of wind power access proportion (0~70%). After exceeding 70%, the transient stability margin decreases with the increase of wind power access proportion. In the case of CMD, the transient stability margin decreases regardless of the proportion of wind power output power. The transient stability margin increases first (about 0~30%), then decreases (30%~50%), then increases (50%~70%), and finally decreases (more than 70%).

The equivalent power angle curve is different when the proportion of wind farm output power changes. Taking the wind power access ratio of 40% as an example, the equivalent power angle curve is shown in Fig. 4. The first swing angle difference under different wind power access ratios is shown in Table IV. Due to the uncertainty of GMD, the first swing angle difference takes the maximum value.

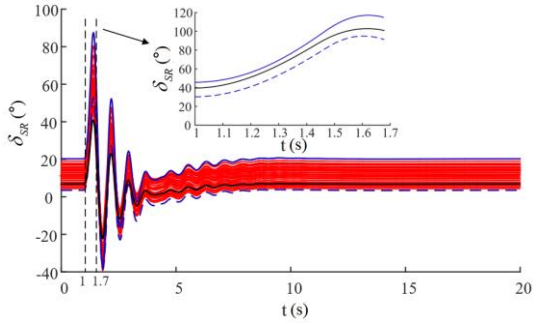

Fig. 4. Equivalent power angle curve

TABLE IV
POWER ANGLE DIFFERENCE OF FIRST SWING

k_S(%)	No GMD	GMD
0	100.5	130.2
10	92.4	111.6
20	84.3	100.4
30	65.3	83.5
40	69.5	89.7
50	84.2	96.5
60	61.3	79.8
70	54.5	67.8
80	96.5	98.3
90	100.1	108.7

For the case without GMD, the power angle difference of the first swing decreases first (the proportion of wind power access is 0~70%) and then increases (greater than 70%). In the case of GMD, the power angle difference of the first swing decreases first (0~30%), then increases (30%~50%), then decreases (50%~70%), and finally increases (greater than 70%). In the case of GMD, the variation of critical clearing angle, first swing angle difference and transient stability margin with the proportion of wind power access are consistent.

V. CONCLUSION

In this paper, through the correlation between the induced geoelectric field, GIC-Q and the equivalent rotor motion equation, it was proved that GMDs could affect not only the voltage stability, but also the transient power angle stability of the system. By quantitatively evaluating the impact of GMDs on transient stability based on the modified IEEE 118-bus test case, conclusions are given as follows:

1) Based on the 29 strong geomagnetic storms in the 23rd solar activity cycle, the induced geoelectric field data was calculated, and the probability distribution analysis and fuzzy feature extraction of distribution parameters were carried out. The results showed that the induced geoelectric field component obeys t location-scale distribution, and its shape parameters, scale parameters and location parameters are fuzzy, but its boundary can be defined within a certain confidence interval to obtain its membership function. Therefore, the induced geoelectric field can be regard as a random fuzzy variable to study the influence of geomagnetic storms on the stability of the power system.

2) The GMDs, an uncertain factor, affects the expected value of critical clearing angle, the expected value of acceleration/deceleration area and transient stability margin. Compared with the case without GMDs, when GMDs occur, the critical clearing angle and transient margin of the system are reduced. When the proportion of wind farm output power reaches about 50%, the transient stability margin of the system is the smallest. Therefore, GMDs can deteriorate the transient stability of the system.

REFERENCES

[1] T. J. Overbye, T. R. Hutchins, K. Shetye, J. Weber and S. Dahman, "Integration of geomagnetic disturbance modeling into the power flow: A methodology for large-scale system studies," in 2012 North American Power Symposium (NAPS), Champaign, IL, USA, 2012, pp. 1-7.

[2] G. P. Juvekar, C. Klauber, K. R. Davis, et al, "GIC-Inclusive State Estimator for Power System Awareness During Geomagnetic Disturbance Events," IEEE Trans. Power Syst., vol. 36, no. 4, pp. 2966-2974, July 2021.

[3] R. P. Jayasinghe, "Investigation of protection problems due to geomagnetically induced current," Ph.D. dissertation, Dept. Elec. Eng., Univ. Manitoba, Winning, MB, Canda 1997.

[4] A. Pulkkinen, S. Lindahl, A Viljanen, and R. Pirjola, "Geomagnetic storm of 29-31 October 2003: Geomagnetically induced currents and their relation to problems in the Swedish high-voltage power transmission system, " Space Weather, vol.3, no.8, August 2005.

[5] A. Haddadi, R. Hassani, J. Mahseredjian, L. Gérin-Lajoie and A. Rezaei-Zare, "Evaluation of Simulation Methods for Analysis of Geomagnetic Disturbance System Impacts," IEEE Trans. Power Deliv., vol. 36, no. 3, pp. 1509-1516, June 2021.

[6] Liu Chunming, Wang Hongmei, Wang Xuan, "Statistical Analysis of Geomagnetically Induced Currents in UHV Power Grids Under Multiple Geomagnetic Storms," Proceedings of the CSEE, vol. 39, no. 15, pp. 4606-4614, August 2019.

[7] A. H. Etemadi and A. Rezaei-Zare, "Optimal Placement of GIC Blocking Devices for Geomagnetic Disturbance Mitigation," IEEE Trans. on Power Syst., vol. 29, no. 6, pp. 2753-2762, November 2014.

[8] Marshall R A, Smith E A, Francis M J, et al, "A Preliminary risk assessment of the Australian region power network to space weather," Space Weather, vol. 9, no. 10, pp. 1-18, October 2011.

[9] Wu Weili, Liu Lianguang, Wang Kairang, "Risk Assessment Methods and Models of Power System Fault Due to Geomagnetic Disturbance," Proceedings of the CSEE, vol. 35, no. 4, pp. 830-839, February 2015.

[10] A. Haddadi, R. Hassani, J. Mahseredjian, L. Gérin-Lajoie et al, "Evaluation of Simulation Methods for Analysis of Geomagnetic Disturbance System Impacts," IEEE Trans. Power Deliv., vol. 36, no. 3, pp. 1509-1516, June 2021.

[11] R. Horton, D. Boteler, T. J. Overbye, R. Pirjola and R. C. Dugan, "A Test Case for the Calculation of Geomagnetically Induced Currents," IEEE Trans. Power Deliv, vol. 27, no. 4, pp. 2368-2373, October 2012.

[12] A. Rezaei-Zare, "Behavior of Single-Phase Transformers Under Geomagnetically Induced Current Conditions," IEEE Trans. Power Deliv., vol. 29, no. 2, pp. 916-925, April 2014.

[13] Jiang Huilan, Zhou Zhaoqing, Cai Jichao, "Analysis method of Influence of Wind Power Access Proportion on Transient Power Angle Stability of Power System," Electric Power Automation Equipment, vol. 40, no. 7, pp. 53-61, July 2020.

[14] A. Haddadi, A. Rezaei-Zare, L. Gérin-Lajoie, R. Hassani and J. Mahseredjian, "A Modified IEEE 118-Bus Test Case for Geomagnetic Disturbance Studies–Part I: Model Data," IEEE Trans. Electromag. Compat., vol. 62, no. 3, pp. 955-965, June 2020.

[15] M. A. M. Ariff and B. C. Pal, "Coherency Identification in Interconnected Power System—An Independent Component Analysis Approach," IEEE Trans. Power Syst., vol. 28, no. 2, pp. 1747-1755, May 2013.